

Direct detection of dark matter

Peter Bosch, Max Briel and Jelle van Urk

June 2018



Contents

1	Introduction <i>MB</i>	4
2	Interaction Rate <i>MB</i>	5
2.1	Form Factor <i>MB</i>	6
2.2	Velocity Distribution <i>JvU</i>	7
2.3	Local Dark Matter Density <i>JvU</i>	9
2.3.1	Newtonian approximation	9
2.3.2	Tracer stars model	9
3	Elastic Scattering <i>MB</i>	12
3.1	Spin-independent	12
3.2	Spin-dependent	13
4	Inelastic Scattering <i>MB</i>	14
4.1	WIMP excitation	14
4.2	Nuclear excitation	15
4.3	Electron excitation <i>MB and PB</i>	15
5	Experiments <i>PB</i>	17
5.1	Three ways to measure	17
5.2	Working principle (scintillation and ionization)	17
5.2.1	Content TPC	18
5.3	Current experiments	18
5.3.1	PandaX-II	19
5.3.2	LUX	19
5.3.3	XENON1T	19
5.3.4	DarkSide	20
5.3.5	SuperCDMS	20
5.3.6	CRESST-II	20
5.4	Future experiments	20
5.4.1	XENONnT	21
5.4.2	DARWIN	21
5.4.3	LZ	21
5.5	Electron excitation detectors	21
5.5.1	Noble liquids	23
5.5.2	Semiconductors	23
6	Neutrino floor <i>PB</i>	24
6.1	Origin of neutrinos <i>PB</i>	24
6.1.1	Solar neutrinos	25
6.1.2	Atmospheric neutrinos	25
6.1.3	Supernovae neutrinos	26
6.1.4	Other neutrinos	26
6.2	A fundamental limit <i>MB</i>	26

6.3	Continue searching? JvU	28
6.3.1	Directional experiments	29
6.3.2	Annual modulation	29
6.3.3	Extraction of neutrino background	30

1 Introduction *MB*

Deviations from the galactic rotation curves and other astrophysical observations provide evidence for the presence of additional unobserved matter: Dark Matter. From the Cosmic Microwave background it has been deduced that this matter cannot be of baryonic nature and accounts for 80% of the matter in the Milky Way, while only interacting gravitationally with ordinary matter [1]. This lead to the idea of the WIMP particle, a Weakly Interacting Massive Particle, as an source of observed gravitational interactions. However, since it's only weakly interacting with ordinary matter, its detection is a difficult task. This can either be achieved using a indirect detection, where products that can only come from Dark Matter interactions are observed. However, the possibility remains for other processes to give the same results.

More concrete evidence can be provided by direct detection of dark matter interacting with standard model matter. A Weakly Interacting Massive Particle is expected to have these interactions through the weak force. Direct detection experiments focus on measuring a recoil effect from collisions of dark matter particles with ordinary matter.

2 Interaction Rate MB

For direct detection experiments to draw conclusions from their measurements, it is important to know the expected rate of WIMP interactions in the detector. Because a WIMP can scatter elastically and inelastically off matter, this section will consider the general components of the interaction rate, while specific properties will be discussed in sections 3 and 4. A simple first approximation of the interaction rate would be an exponentially decay with recoil energy (E_R) with dependencies on the WIMP mass (m_χ) and detector particle mass (m_T).

$$\frac{dR}{dE_R} = \frac{R_0}{E_0 r} e^{-E_R/E_0 r}, \quad \text{with } r = \frac{4m_\chi \cdot m_T}{(m_\chi + m_T)^2}, \quad (1)$$

where E_0 the most probable dark matter kinetic energy, and R_0 the total event rate [2]. This is a extremely crude approximation for the expected number of events, which neglects important details in the interaction rate curve. Lewin and Smith provide an overview of corrections to the rate [2].

First of all, the movement of the Earth and Sun through the Galaxy alter the rate at which the dark matter particles go through the Earth [3]. Assuming a isotropically dark matter distribution in our Galaxy, the dark matter flux increases when the Earth moves into the same direction as the Sun and vice versa. This will be discussed further in section 2.3 and 2.2.

Secondly, properties of the detector alter the number of interactions that are expected. These range from more practical aspects, such as the resolution of the photomultipliers, to the type of material used in the detector. Moreover, the efficiency with which nuclear and electronic recoil events can be distinguished determines the accuracy of the measured rate at a recoil energy.

Furthermore, the WIMP interaction can be dependent on the spin. Spin-independent interactions provide a stronger signal due to its scalar nature and coherent nature at low energies. And finally, due to the particle wavelength being smaller than the radius of the target a correction to the cross section has to be applied, called the form factor. These corrections are combined to form a complete picture of the interaction rate per kg detector material (Eq. 2) [2, 4].

$$\frac{dR}{dE_R}(E, t) = \frac{\rho_0}{m_\chi \cdot m_T} \int_{v_{\min}}^{v_{\max}} v \cdot f(\mathbf{v}, t) \frac{d\sigma}{dE_R}(E, v) d^3v, \quad (2)$$

where ρ_0 is the local dark matter density, $f(\mathbf{v}, t)$ the velocity distribution of dark matter particles, and $\frac{d\sigma}{dE}$ its differential cross section through which the particle physics enters, such as the cross section and form factor, which can depend on the spin. σ_0 is the cross section at zero momentum and depends on the type and spin dependence of the interaction.

$$\frac{d\sigma}{dE_R} = \frac{m_T}{2\mu_T^2 v^2} (\sigma_0^{\text{SD}} F_{\text{SD}}^2(E_R) + \sigma_0^{\text{SI}} F_{\text{SI}}^2(E_R)) \quad (3)$$

Furthermore, it is important to note that the differential interaction rate has a dark matter mass dependence of $1/m_\chi$. Because of this the interaction rate of a

high WIMP mass is smaller than for lower masses. However, at too low masses the energy of the WIMP is not high enough to be detected. Therefore, the interaction cross section becomes harder to measure in these regimes. This results in the typical shape of the detection limits as shown in figure 12 in section 5.3 for several detectors.

2.1 Form Factor MB

During the collision momentum is transferred between the particles. If this momentum exchange is extremely small, its wavelength can be smaller than the radius of the particle. This results in loss of coherence and a decrease in the effective cross section, which is implemented by the form factor. The spin-independent form factor is calculated using a Fourier transform of the scattering centres assuming they follow the same distribution as the charge density [2]. Since this involves an integral that has to be numerically solved, it is more common to use the Helm form factor, which is an analytical approximation [5].

$$F_{SI}^2 = \left[\frac{3j_1(qR_1)}{qR_1} \right]^2 e^{-q^2 s^2}, \quad (4)$$

where j_i is the spherical Bessel function of the first kind and $q = \sqrt{2m_T E_R}$ the momentum transfer. The other variables determine the parametrisation and come from spectroscopy experiments [6]. Shell-model [7] and Hartree-Fock calculations [8, 9] have shown that the Helm parametrisation deviates the total event rate less than 5%. Furthermore, equation 4 shows that the form factor suppresses the event rate at high recoil energies. This is more present with high mass target particles, because σ_0 has a quadratic dependence on its mass number, increasing the form factors effect [4]. To determine the spin-dependent form factor the type of scattering particle has to be determined. For an interaction with a nucleus the form factor can be rewritten as a normalised response function of an ensemble of spin-1/2 particles.

$$F_{SD}^2 = \frac{S(E_R)}{S(0)} \quad (5)$$

The response function consists of spin-structure functions [10], which are often calculated using nuclear shell-models [11, 12], but other atomic models can lead to different spin structure functions [13–15].

$$S(E_R) = a_0^2 S_{00}(E_R) + a_0 a_1 S_{01}(E_R) + a_1^2 S_{11}(E_R), \quad (6)$$

Cerdeño et al.[16] proposed a parametrisation that mimics the median value of a collection of spin structure calculations to solve this problem.

$$S_{ij} = N((1 - \beta)e^{-\alpha u} + \beta), \quad (7)$$

where α , N , and β are parameters determined from measurements, while $u = (qb)^2/2$ consists of q , the momentum transfer and b as shown in equation 8.

$$b = \sqrt{\frac{41.467}{45.0A^{-1/3} - 25.0A^{-2/3}}} \quad (8)$$

The WIMP particle could also scatter off an electron. Since the electron is in a bound state, two competing processes affect the effective cross section. This results in a more complex form factor consisting of a Sommerfeld enhancement [17] and suppression from the need to overcome the binding energy [18]. More details mathematics for the calculation of WIMP interactions have been proposed, such as non-relativistic Effective Field Theory [19]. This could give a better description of the effective cross section of the collision and possibly make it impossible to compare direct detection experiments with different target material [20].

2.2 Velocity Distribution JvU

As mentioned in the previous section, the scattering rate depends on an integral over the velocity distribution $f(\mathbf{v}, t)$ of the DM particles. These particles tend to be moving in an isotropic Maxwellian distribution around 0 inside in the DM halo. The distribution is shifted due to the movement of the Earth through the DM halo, which is built up from the rotation of the galaxy at the location of the Sun ($220 \frac{\text{km}}{\text{s}}$), the Earth's movement around the Sun ($30 \frac{\text{km}}{\text{s}}$) and the rotation of the Earth. The time dependence comes from the fact that the velocity of the Earth is not constant over the course of a year. However, this time dependence and the Earth's rotation are small contributions to the total velocity and are often neglected. In figure 1 three different high resolution simulations of the velocity distribution are shown [21].

As the distribution is assumed to be Maxwellian, it has the following expression for calculating the scattering rate [22]:

$$f(\mathbf{v}) = \frac{1}{(\pi v_{\text{Earth}}^2)^{\frac{3}{2}}} e^{(-\frac{\mathbf{v}^2}{v_{\text{Earth}}^2})}, \quad (9)$$

where v_{Earth} is the average velocity of the Earth through the DM halo, around $250 \frac{\text{km}}{\text{s}}$. The next important part is determining the integration bounds of equation 2. The lower bound depends on the sensitivity of the detector. The WIMP's need a certain velocity that results in a recoil energy high enough for the detector to measure it (v_{\min}), given by [23]:

$$v_{\min} = \sqrt{\frac{m_T E_R}{2\mu_{\chi T}^2}}. \quad (10)$$

In the expression μ_T is the reduced mass of the WIMP and target nucleus and E_R is the minimum recoil energy that the detector needs. The upper bound of the integral is the local escape velocity of the galaxy (v_{esc}). This velocity lies between $498 \frac{\text{km}}{\text{s}}$ and $608 \frac{\text{km}}{\text{s}}$ [24].

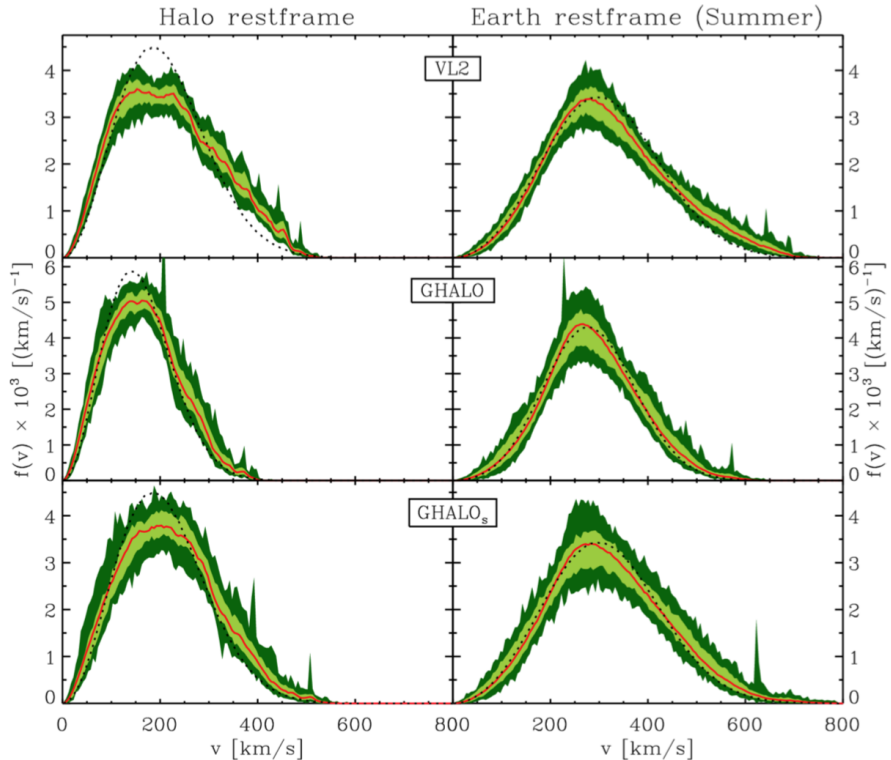


Figure 1: Three high resolution simulations of the velocity distribution of the WIMPs in the neighbourhood of the Sun [21]. On the left side only the movement of the galaxy is taken into account ($220 \frac{km}{s}$), the right figures also added the Earth's orbit ($30 \frac{km}{s}$). The shape of the distribution is close to being Maxwellian and therefore the $f(\mathbf{v}, t)$ is approximated by a Maxwell-Boltzmann distribution.

2.3 Local Dark Matter Density JvU

To get a better insight in the scattering interaction rate it's important to have some measurements in the local dark matter density (ρ_{DM}), because $\frac{dR}{dE_R}$ is directly proportional to this density. The local DM density gives the density in close neighbourhood of the SUN, usually around 100 - 1000pc. Older measurements give an local density of $0.542 \pm 0.042 \frac{\text{GeV}}{\text{cm}^3}$ [25] and $0.25 \pm 0.09 \frac{\text{GeV}}{\text{cm}^3}$ [26]. Clearly they're not even similar within their uncertainties. Mainly because both used different data sets and assumptions in their methods. Therefore new calculations are done with the least amount of assumptions. In the next sections we will describe two of those methods. The first is a global measure, which divides the DM halo into substructures and simulates the way they interact. The second uses the vertical motion of nearby stars, also called 'tracers' [27]. These motions are described with Jeans equations.

In figure 2 a history of local DM density measurements is shown over the last century. The first measurement was done by Kapteyn in 1922, who was the first who claimed to have proved the existence of dark matter. However, in the following decades his method was corrected and extended. In the late 80's there was a boost in the measurements, since new satellites were able to look at around 100.000 stars in a 100 pc radius. The different colors in the circles point out a different method used to determine the density: the values in blue are calculated from a surface density, the red one used the rotation curve and the green circle used a different assumption on the surface density [27]. The grey band is $\rho_{DM,ext}$, the extrapolation of the rotation curve.

2.3.1 Newtonian approximation

The first method divides the DM halo into smaller substructures (superparticles), and numerically simulate the way they grow and interact with each other. These masses given to these superparticles lie around $10^3 M_\odot$. These simulations integrate and solve the equations of motion of the Newtonian gravity between N superparticles. A comprehensive explanation of this 'Newtonian' approximation is elaborated in this article [28].

This method starts with Dark Matter Only (DMO) simulations. These simulations already give a good representation of some of the properties of the DM halo, like the shape and the local DM density of the halo. It's also in agreement with the simulations of the velocity distribution in figure 1, as it predicts the distribution to be near Maxwellian [27]. The second step is including baryons to the simulations. We know that most matter close to the Sun in the disc plane of the Milky Way mostly consist baryonic matter. As a consequence this changes ρ_{DM} quite significantly in the simulations [27].

2.3.2 Tracer stars model

The second method uses the vertical movement of neighbouring stars, also known as 'tracer stars'. In this system the stars obey the collisionless Boltzmann

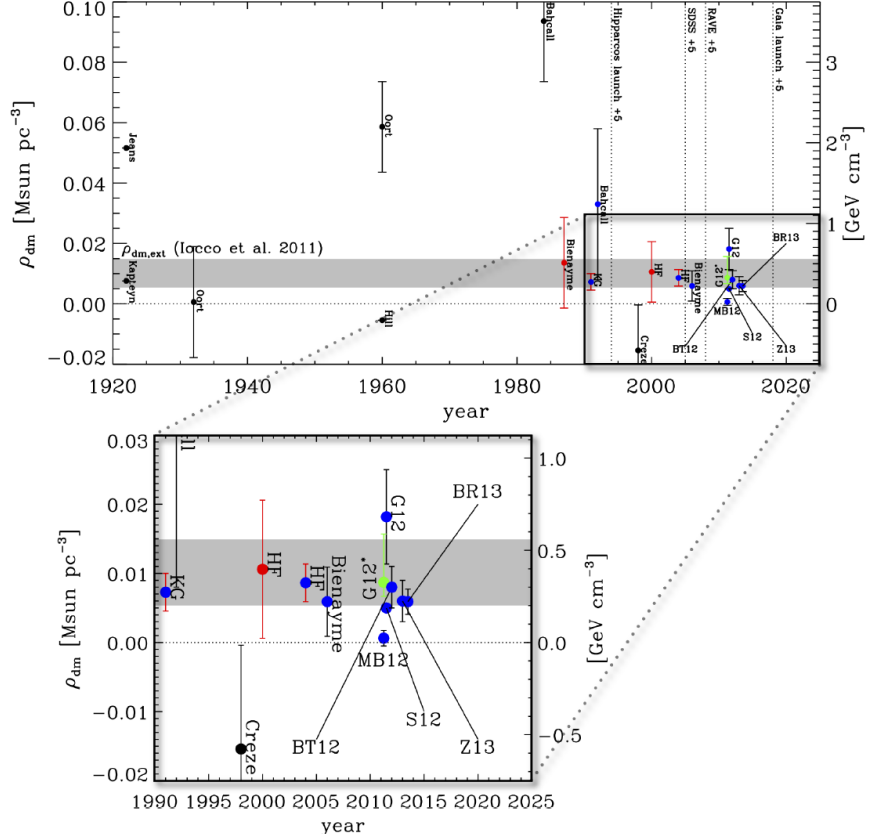


Figure 2: Measurements of ρ_{DM} over the past 100 years [27]. The grey band is an extrapolation of the rotation curve, $\rho_{DM,ext}$. The different colored circles use different methods to determine the local DM density.

equation:

$$\frac{df}{dt} = \frac{df}{dt} + \nabla_x f \cdot \mathbf{v} - \nabla_v f \cdot \nabla_x \Phi = 0, \quad (11)$$

where f is the distribution function of the surrounding stars. \mathbf{v} and \mathbf{x} are their velocity and position. The remaining Φ corresponds to the gravitational potential. If the system was in dynamical equilibrium, which isn't the case, we could directly calculate the gravitational forces between the stars. For our purposes we need to integrate this equation, which results in the Jeans equations [29]. We are interested in the z-direction of the tracers, because their vertical movement is mostly induced by the gravitational force of the DM particles in the halo. That's because all the baryonic matter lies in the disc plane of the galaxy and the density quickly decreases in the z-direction. For this reason we

take the vertical component of the Jeans equation [25]:

$$\frac{1}{R\nu} \frac{\partial}{\partial R} (R\nu\sigma_{Rz}) + \frac{1}{R\nu} \frac{\partial}{\partial \phi} (\nu\sigma_{\phi z}) + \frac{1}{\nu} \frac{d}{dz} (\nu\sigma_z^2) = -\frac{d\Phi}{dz}, \quad (12)$$

where the first term is the 'tilt' term (T). This term couples the vertical and radial motion of the tracers. The second term is the 'axial' term (A), which does the same for the vertical and axial motions. The right hand side of this equation is the vertical acceleration K. Integrating both sides with respect to z gives us the necessary expression for σ_z^2 , which is the vertical velocity dispersion:

$$\sigma_z^2(z) = \frac{1}{\nu(z)} \int_0^z \nu(z') [K_z(z') - T(z') - A(z')] dz' + \frac{C}{\nu(z)}. \quad (13)$$

Knowing the vertical velocity distribution of the tracers, it's possible to calculate ρ_{DM} necessary to induce this movement. The complete method and calculations are beyond the scope of this report and are derived in [29], which leads to some interesting results. They numerically simulate the different terms in equation 12, where they also show the importance of the 'tilt' term.

3 Elastic Scattering MB

The two main interaction mechanism between WIMPS and ordinary matter are elastic and inelastic scattering. The idea for elastic scattering of Dark Matter was introduced in 1984 by Goodman & Witten [30] and can produce a nuclear recoil effect necessary for measurement, while the momentum is conserved [2, 4]. This can take place in a spin-dependent and spin-independent fashion.

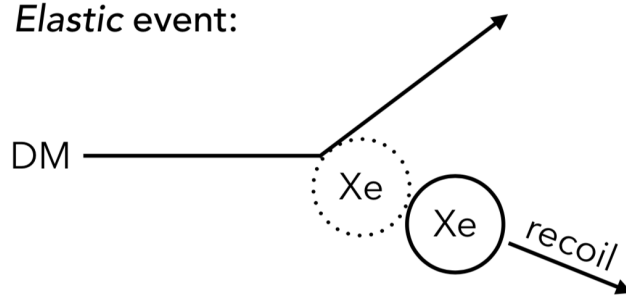


Figure 3: Dark matter particle elastically scattering of a Xenon atom that recoils due to the collision. Image from [31].

3.1 Spin-independent

In a WIMP scenario it is expected that spin-independent interactions provide the largest contribution to the effective cross section. This becomes clear if the cross section at zero momentum from equation 3 is written out.

$$\sigma_0^{\text{SI}} = \sigma_{p\chi} \frac{\mu_T^2}{\mu_p^2} [Z \cdot f^p + (A - Z)f^n]^2 \quad (14)$$

There is a contribution to the WIMP interaction from the protons and neutrons in the nucleus with an interaction cross section between the WIMP and a proton $\sigma_{p\chi}$. Although other theories exists [32], it is assumed in most cases that the interaction strength from the protons and neutrons with the WIMP are equal ($f^n = f^p$). This results in a A^2 dependence, where A is the atom mass number. This enhancement is of the order $\sim 10^4$ [7] and, therefore, heavy mass atoms are used as a target material in most direct detection experiments. However, the heavier mass number also increases the influence of the form factor on the event rate, which can cause a significant drop in interactions, as shown in figure 4. Thus, different detectors can be sensitive in different regions. The spin-independent part can also completely vanish depending on the assumed nature of the WIMP particle [2].

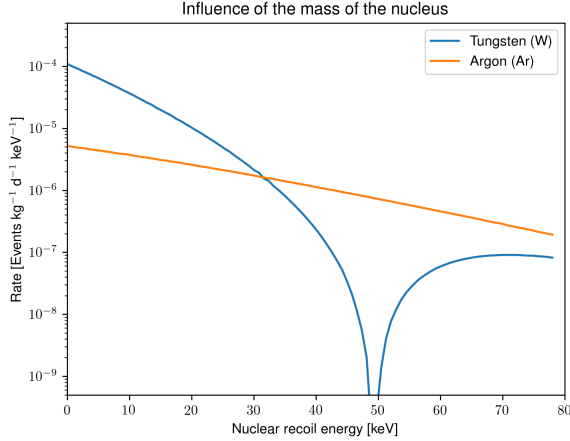


Figure 4: The mass number of the target material alters the interaction rate by increasing the influence of the form factor. The data comes from [4] with a WIMP mass of $100 \text{ GeV}/c^2$ and a cross section of 10^{-45} cm^2 .

3.2 Spin-dependent

It is unknown if a dark matter particle can even spin-independently scatter off a nucleus. Therefore, researchers also have to look at a possible spin-dependent interactions. Depending on the theory, this interaction strength could be stronger than spin-independent scattering. However, if it is assumed that the nucleon-WIMP cross section is equal for both types, the spin-independent cross section will dominate due to its A^2 dependence as mentioned in section 3.1.

The corresponding zero momentum cross section of spin-dependent scattering is often expressed in average spin interaction $\langle S \rangle$ between the WIMP and neutrons & protons.

$$\sigma_0^{\text{SD}} = \frac{32}{\pi} \mu_T^2 G_F^2 [a_p \langle S^p \rangle + a_n \langle S^n \rangle]^2 \frac{J+1}{J}, \quad (15)$$

which depends on the total nuclear spin (J), Fermi coupling constant (G_F^2), and the effective coupling between the WIMP and nucleon particles (a_p & a_n) [4]. The latter are often assumed to be the same [22] and can be calculated using chiral effective field theory currents [33] or shell-model calculations [12].

4 Inelastic Scattering MB

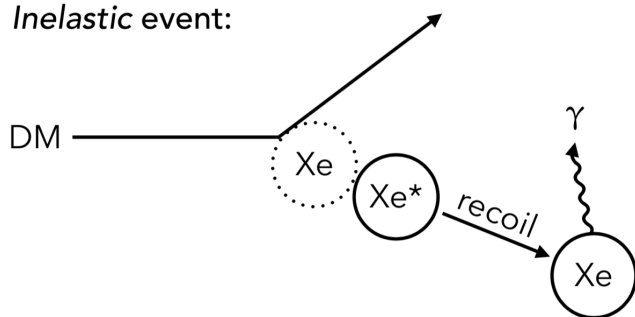


Figure 5: A dark matter particle scattering inelastically off a Xenon atom, which recoils and is put into an excited state. This is followed by a de-excitation and the emission of a photon. Image from [31].

Another possible interaction channel is inelastic scattering of the WIMP, during which one of the particles is excited, because the average recoil energy of the interaction is around 1-100 keV. This is in the range for excitation of nuclear excitation, allowing it to be a candidate channel for dark matter detection [30, 34]. In the detector, three possible particles can be excited: an electron [35], the nucleus [34], or the WIMP [36–38]. While these have each their own properties, they require a larger minimal dark matter velocity [36] and can be spin-dependent [31] or spin-independent. It is important to note that other mechanisms, ideas, and particles have been proposed [4, 37, 39, 40] as the dark matter particle, but these are, currently, not in the spotlight of research [41].

$$v_{\min} = \frac{1}{\sqrt{2m_T E_R}} \left(\frac{m_T E_R}{\mu_{T\chi}} + \delta \right) \quad (16)$$

4.1 WIMP excitation

One of the excited particles can be the WIMP particle. This channel was introduced by Tucker-Smith and Weiner in 2001 [36] to explain discrepancies between DAMA [42] and other direct detection experiments [43, 44]. The idea is that dark matter particles with enough kinetic energy up scatter into the heavier excited state above the threshold energy for this interaction, altering the relative sensitivity of detectors in three ways [36, 37, 43]:

- **Suppression of low-energy events** Dark matter particles mostly have low velocities. Thus, they do not have the energy to excite the WIMP, making it impossible to detect this range of energies.

- **Annual modulation enhancement** When the earth moves in the same direction as the sun the velocity distribution is shifted upwards, allowing for more inelastic scatterings. However, if the earth moves in the opposite direction, then distribution is shifted downwards and less particles are above the threshold energy for excitation.
- **Heavier elements are favoured** With a heavier target mass material the WIMPs have a larger velocity range available to scatter off. Therefore, detectors with such heavier elements would be favoured in the inelastic scattering case.

This mechanism has been experimentally constraint by the XENON [45], CDMS [46], and ZEPLIN [47] collaborations.

4.2 Nuclear excitation

Another possibility is the excitation of the nucleus followed by a de-excitation. This can be induced in odd-mass nuclei [48]. Since natural xenon contains odd and even isotopes, experiments using xenon can probe both elastic and inelastic scattering [31]. The XENON100 and XMASS collaborations have set upper limit on this spin-dependent inelastic nucleon-WIMP interaction to $3.3 \times 10^{-38} \text{ cm}^2$ [49, 50]. If this interaction is detected, it provides proof for the spin-dependent nature of the WIMP-nucleon interaction.

4.3 Electron excitation *MB and PB*

A final option is the excitation of an electron in the interaction. This can lead to an ionization of the atom [18], which requires an energy transfer of 1-10 eV. This is in the recoil energy ranges of light dark matter particles with masses of keV to MeV. Such energies would be insufficient for nuclear recoil to take place. Thus, inelastic electron-WIMP scattering is essential to probe the lower mass region of the WIMP parameter space. Using this mechanism four different methods can be used to make measurements. First, an individual electron can be measured that has been kick out of the atom by the dark matter particle [51–53]. From this interaction it is also possible to measure the leftover ion. left over energy after the ionisation can be send out as heat in the form of phonons. This might be possible using ultra-low threshold detectors [54]. Furthermore, it is possible to measure the photon emitted in the de-excitation phase. This is not an easy task, because it requires a good understanding of the atomic structure of the target material and a photon must not be in resonance for re-absorption [35]. In current searches in the sub-GeV WIMP mass regime the main method for detecting an electron-WIMP interaction is ionization of the target atom.

Just like before, also here an interaction rate can be calculated. This interaction rate for electron recoils is

$$\frac{dR_{ion}}{d \ln E_R} = N_T \frac{\rho_\chi}{m_\chi} \frac{d \langle \sigma_{ion} v \rangle}{d \ln E_R} \quad (17)$$

with N_T the number of target nuclei per unit mass in the detector and $\frac{d\langle \sigma_{ion}^i v \rangle}{d \ln E_R}$ is

$$\frac{d\langle \sigma_{ion}^i v \rangle}{d \ln E_R} = \frac{\bar{\sigma}_e}{8\mu_{\chi e}^2} \int q \, dq |f_{ion}^i(k', q)|^2 |F_{DM}|^2 \eta(v_{min}) \quad (18)$$

where i is the energy level the electron is in and $f_{ion}^i(k', q)$ is the electron's ionisation form factor. For a detailed description of this, see e.g. [18].

5 Experiments *PB*

Several experiments are operational to detect dark matter directly. In this section the working principle of these detectors, the current experiments and the experiments planned for in the future are discussed.

5.1 Three ways to measure

Three things can be measured to detect dark matter:

- scintillation,
- ionization and
- heat.

For direct dark matter detectors it is an advantage to measure a combination of two of them. In this way electron recoils can be discriminated from nuclear recoils. The ratio between the so-called S1 and S2 signals (see section 5.2) can tell whether it was a nuclear or electron recoil [55]. The detectors in sections 5.3.1 till 5.3.4 use scintillation and ionization. The SuperCDMS detector in section 5.3.5 detects heat and photons (scintillation). In CRESST (section 5.3.6) heat and ionization is measured. As most leading detectors use dual-phase xenon TPCs, only this will be covered in more detail (for dual-phase xenon TPCs and other detection principles, see [55]).

5.2 Working principle (scintillation and ionization)

Some of the WIMPs in the universe are directing towards Earth. It is barely interacting with ordinary matter and will reach Earth. There it goes through the atmosphere (without interacting). At the surface it is still not interacting and comes into the underground observatories. At these observatories detectors are placed in big tanks of water to prevent other particles to enter the detector. The used detectors are Time Projection Chambers (TPCs) [56]. The WIMP is interacting with the molecules in the TPC. Some light is created and detected with photomultipliers (S1 signal). The electrons created in the interaction are drifted by an external electric field. When reached the top of the detector, lots of photons are created and detected (S2 signal). A second signal is measured to be able to get the z-position of the interaction. This can be done with the time difference between the S1 and S2 signal. To reduce background, the detectors are placed in basins of e.g. water. Non-dark matter particles will interact in here before entering the TPC. In this way interactions between WIMPs and the molecules of the TPC can be detected. This is sketched in figure 6.

With this process, the cross section of the interactions of WIMPs and the molecules of the TPC can be determined. So far, only upper limits of the cross section are found in several experiments (see figure 12). Some of the existing experiments are covered in section 5.3.

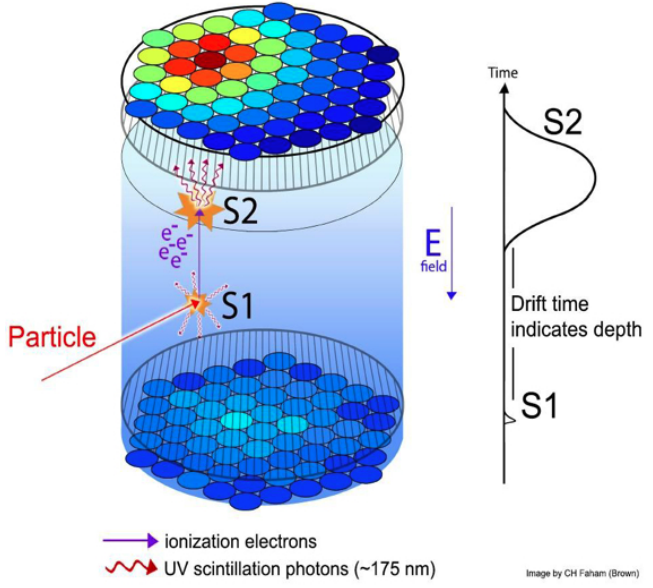


Figure 6: Working principle of a dual-phase DM detector [56]. A (dark matter) particle enters the detector. When it interacts, a some light is created. This light is detected at the top and bottom of the detector (S1 signal). The electrons that were created in the interaction start drifting due to a external electric field. When the electrons start to enter the gaseous part of the detector, a bunch of light is created (S2 signal). This will again be measured. These measurements will give a two dimensional reconstruction of the place where the interaction happened. The time difference between S1 and S2 due to the “finite” drift velocity can give the third dimension.

5.2.1 Content TPC

One can chose the material inside the TPC. Mostly liquid noble-gasses are used. Xenon is the most used noble-gas, although also argon is being used. The advantage of using xenon is that it is sensitive to both spin-dependent and spin-independent interactions [57], it is self-shielding due to a high density (so more xenon can be used for measuring) [4] and it is stable. The greatest part of the xenon in the detector is in the liquid phase. On the top some gaseous xenon creates the S2 signal [55].

5.3 Current experiments

At the moment, several experiments on the direct detection of dark matter are being done. Some of them are discussed here: the PandaX-II detector in

Sichuan, China, the LUX detector in South Dakota, USA and the XENON1T detector in Abruzzo, Italy.

5.3.1 PandaX-II

Particle and Astrophysical Xenon Detector II (PandaX-II) is a dark matter experiment situated in the region Sichuan in the People's Republic of China. It is a detector with 300 kg of effective liquid xenon target [58] (more details and latest results in e.g. [59]).



Figure 7: A detail of the PandaX-II detector [60].

5.3.2 LUX

The Large Underground Xenon experiment (LUX) in the Sanford Underground Research Facility near Lead, South Dakota, USA is an 30 million US dollar costing experiment looking for dark matter at 1,480 meters depth [61]. The latest results are written in [62]. For more details see e.g. [63].

5.3.3 XENON1T

In the Gran Sasso d'Italia - a mountain massive in Southern Italy - several scientific experiments are being done. One of them is the XENON1T dark matter detector. 1.3 tonne of liquid xenon is used to take the latest data [65]. Currently, it is the most sensitive dark matter detector (see figure 12). It set the upper limit for the WIMP-nucleon spin-independent cross section for WIMPs with mass $m_\chi = 30 \text{ GeV}/c^2$ at $\sigma_\chi^{m=30 \text{ GeV}/c^2} < 4.1 \times 10^{-47} \text{ cm}^2$.



Figure 8: Inside the LUX detector [64].

5.3.4 DarkSide

Next to the XENON1T experiment the DarkSide experiment is running in the Gran Sasso National Laboratory. This is a direct dark matter detector with TPCs based on argon [67–69]. This detector is a few orders of magnitude less sensitive than the detectors with xenon-based TPCs (see figure 12).

5.3.5 SuperCDMS

In the Soudan Underground Mine, Minnesota, a dark matter detector named SuperCDMS (**S**uper **C**ryogenic **D**ark **M**atter **S**earch) is build (see figure 10). This detector works with silicon crystal cooled down to 33 mK to measure phonons (heat) [41]. More on SuperCDMS in [70–72].

5.3.6 CRESST-II

The **C**ryogenic **R**are **E**vent **S**earch with **S**uperconducting **T**hermometers-II is detecting dark matter with photons and phonons [74]. In this experiment a CaWO_4 crystal is used. Most of the energy deposition is in the form of heat. Less than 5% of the energy goes into the scintillation. For more information on CRESST, see [75–77].

5.4 Future experiments

In the search for dark matter particles one tries to bring down the sensitivity curves (as in figure 12). This is being done with upgrades of existing experiments

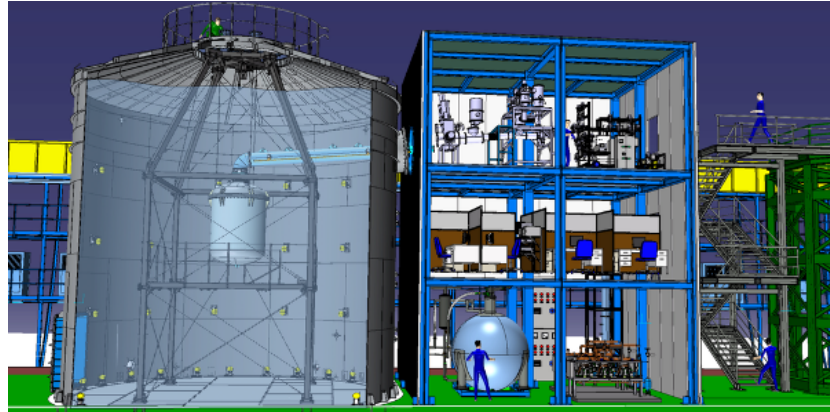


Figure 9: Schematic drawing of the XENON1T detector [66].

and building new detectors. Some of them are discussed in this section.

5.4.1 XENONnT

The XENON collaboration is working on XENONnT as upgrade of the XENON1T experiment. It is going to be a 5.9 tonne sister of the XENON1T detector [65]. The planning is to be running in 2019 [80].

5.4.2 DARWIN

DARWIN is a new to build dark matter detector. DARWIN stands for **D**ark matter **W**IMP search with **N**oble liquids. It will mainly search for WIMPS until the neutrino floor is reached (for the neutrino floor, see section 6) [81]. Also research on axions, the low-energy solar neutrinos and galactic supernovae will be preformed.

5.4.3 LZ

LZ is a combination of LUX and ZEPLIN (**Z**oned proportional scintillation in **l**iquid **n**oble gases). It's currently being built in the Sanford Underground Research Facility. See for more (technical) information [82, 83].

5.5 Electron excitation detectors

For electron excitation less energy is needed compared with nuclear recoils [84]. If an electron is excited, this can be measured just like before with WIMP-nucleus reactions. The only problem with this is that the detectors mentioned before are not very (or even totally not) sensitive for these low energy interactions. To be more sensitive the material inside the detector is often changed. Semiconductors are a good choice to use. This is due to their lower threshold

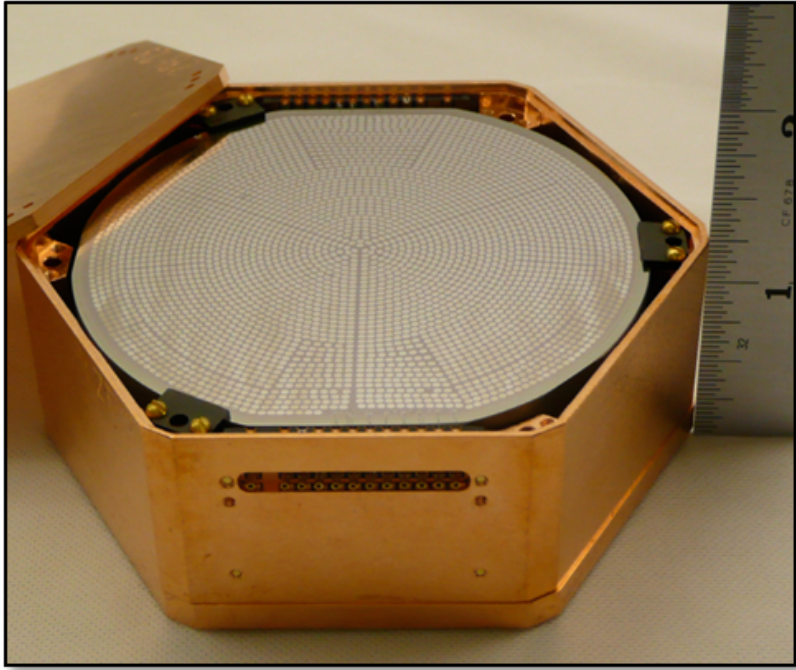


Figure 10: One of the modules used in the SuperCDMS detector [73].



Figure 11: Installation of CRESST [78].

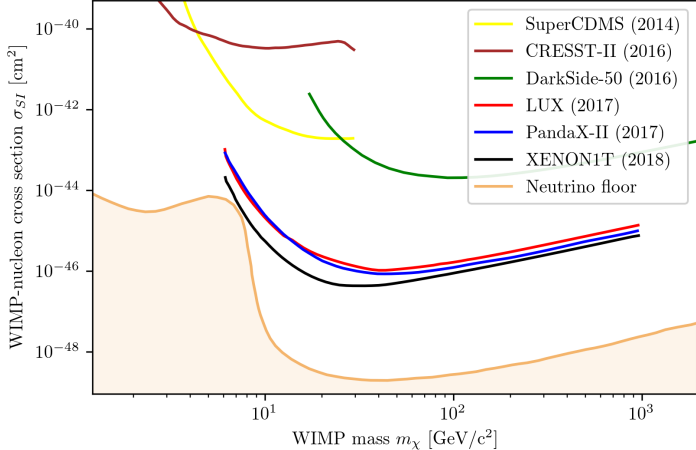


Figure 12: Sensitivity plot of the detectors given in section 5.3. Data from SuperCDMS [71], CRESST-II [74], DarkSide [67], LUX [62], PandaX [59], XENON1T [65] and the neutrino floor [79].

energies. The minimal energy to get ionized is for semiconductors as germanium and silicon 2.9 eV and 3.6 eV while for xenon this is 13.8 eV [85].

5.5.1 Noble liquids

The detectors that work with noble liquids can also detect interactions with electrons and dark matter [18]. Precursors of the detectors given above have already done this (e.g. XENON-10 [86] and ZEPLIN [87]).

5.5.2 Semiconductors

DAMIC The Dark matter in CCD experiment is a dark matter search located at the SNOLAB laboratory in Sudbury, Canada. It makes use of silicon to detect electron recoils with a WIMP mass of $m_\chi < 10 \text{ GeV}/c^2$ [88]. Currently an upgrade is planned, DAMIC-M. This will have a total mass of 1 kg [89].

SENSEI Recently, the Sub-Electron-Noise Skipper CCD Experimental Instrument has published their first results on sub-GeV WIMP search with a prototype detector [90]. In this research again silicon is used. They focused on WIMPs with masses between 500 keV/c 2 and 4 MeV.

6 Neutrino floor *PB*

In dark matter direct detection experiments, one always tries to bring down the sensitivity of interaction in the detector. At a certain moment interactions of neutrinos can not longer be neglected. Although neutrinos have a very small cross section, they do interact. So one will measure the neutrinos in the detector. This is called the neutrino floor. In figure 12 the neutrino floor is given. The yellow solid line is the place where one interaction has taken place. So beneath this line, interactions with neutrinos can become a problem. In this section we will go into the neutrino floor and how to go beneath it.

	Predicted Flux	Energy (MeV)
Solar ν pp	5.99×10^{10}	<0.4
Solar ν CNO	5.46×10^8	<2
Solar ν ^7Be	4.84×10^9	03, 0.8
Solar ν ^8B	5.69×10^6	<12
Solar ν h.e.p.	7.93×10^3	<18
Geo $\bar{\nu}$ ^{238}U	2.34×10^6	<5
Geo $\bar{\nu}$ ^{232}Th	1.99×10^6	<2.5
Geo $\bar{\nu}$ ^{235}U	$\sim 4 \times 10^3$	<2
Geo $\bar{\nu}$ ^{40}K	$\sim 1 \times 10^7$	<2
Atmospheric $\nu + \bar{\nu}$	$O(1/E(\text{GeV})^{2.7})$	0-10 ³
Reactor $\bar{\nu}$	$O(1 \times 10^{20} / \text{distance}^2)$	<10
Supernova Relic $\bar{\nu}$	$O(10^1)$	<60

Table 1: Neutrino fluxes in $\text{cm}^{-2} \text{s}^{-1}$, the energy range and their sources [91].

6.1 Origin of neutrinos *PB*

As said before neutrinos are interacting inside the detectors. These neutrinos are coming from several sources. The main sources are

1. the Sun,
2. the Earth,
3. the atmosphere,
4. supernovae and
5. nuclear reactors.

The neutrino fluxes for these source are given in table 1. Here also the energy range of the neutrinos are given. Different energies will give different recoil spectra in the detectors. For example, ^8B solar neutrinos are affecting measurements on low mass WIMPS (around $m_\chi = 6 \text{ GeV}/c^2$) [92].

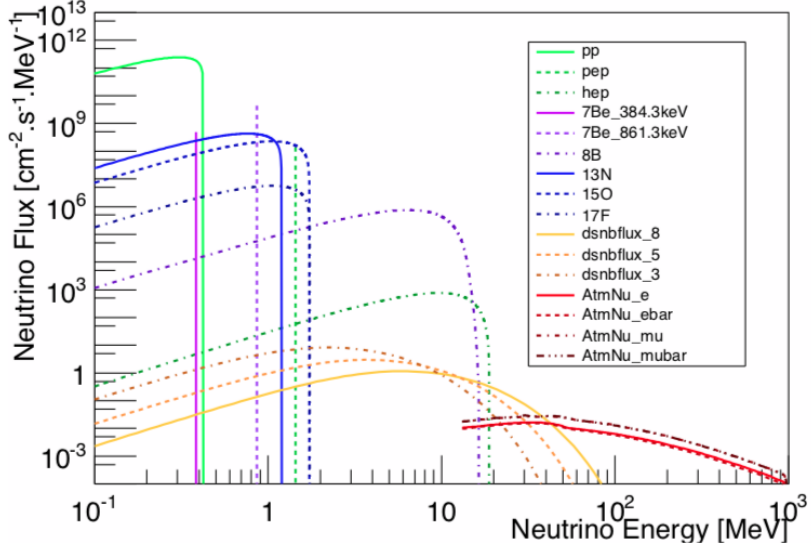
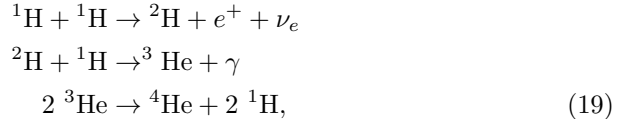


Figure 13: Solar (pp till ^{17}F), diffuse supernova neutrino (dsnbflux) and atmospheric (AtmNu) fluxes arriving at Earth [92].

6.1.1 Solar neutrinos

In the core of the Sun lots of nuclear fusion reactions happen. The main reaction cycle of the Sun is the proton cycle, but also other cycles as the CNO cycle provides the Sun energy [93]. With some of these reactions neutrinos are created. For example, in the full proton-proton cycle,



two neutrinos are created. These neutrinos will travel from the core to the outer shell of the Sun without having any reaction (or at least very little). From there they travel through space. Some of the neutrinos - $2\pi R_\oplus^2 / 4\pi d^2 \approx 10^{-7}\%$ - are going towards Earth. They can also go through the Earth atmosphere without a negligible amount of interactions. Again a small fraction of the remaining neutrinos are hitting the detector in the experiments searching for dark matter. Here the neutrinos interact more because the detectors are made very sensitive for this kind of interactions as they are similar for dark matter interactions.

6.1.2 Atmospheric neutrinos

In the universe particles are created (e.g. pions). These particles move through space without interacting and are called cosmic rays. In the outer atmosphere

pions start to decay creating neutrinos [94, 95]. This is dominated by the decays

$$\pi^+ \rightarrow \mu^+ + \nu_\mu \quad (20)$$

and

$$\mu^+ \rightarrow e^+ + \bar{\nu}_\mu + \nu_e. \quad (21)$$

As before with solar neutrinos, they don't interact in the remaining atmosphere. The non-neutrino particles will further decay and create neutrinos. All these neutrinos can interact in a dark matter detector.

6.1.3 Supernovae neutrinos

At the end of their lifetime, starts explodes [96]. These explosions are called supernovae. Some supernovae create neutrinos [97]. The first neutrinos were detected in 1987 with Kamiokande [98]. The neutrinos were coming from a supernova called SN1987A in the Large Magellanic Cloud.

6.1.4 Other neutrinos

As stated before and can be seen in table 1 there are, besides solar, atmospheric and supernovae neutrinos, two other sources of neutrinos. Some are coming from natural decays in the inner Earth (mostly ^{238}U and ^{232}Th). Also some neutrinos are created by man-made decays in nuclear reactors.

6.2 A fundamental limit MB

It is expected that the neutrino floor will be reached in the coming years; rather sooner than later. This rises the question whether the neutrino background could limit the possible detection of dark matter, because their signal could look like a WIMP particle in current detectors [92, 99]. Due to their extremely small interaction cross section, neutrinos cannot be shielded from the detector. Thus, they impose a limit on the minimum measurable cross section. This is not a final limit; by increasing the exposure, which depends on the mass and measurement time, it is possible to increase the discovery reach. As shown in figure 14, initially, this scales as $1/MT$, when neutrino interactions are minimum. However, at higher exposures the neutrinos become more important and the discovery limit starts to scale as $1/\sqrt{MT}$. The point where it changes is WIMP mass dependent and is often what is called the neutrino floor. In reality it is still possible to continue the exposure and continue the search below this neutrino limit, therefore, it is a "soft" limit. If the exposure is increased even more, eventually the discovery reach will almost flatten out. This plateau is also known as the "hard" floor, but to reach it the exposure has to be unrealistically high [100].

An important part in signal analysis is distinguishing between nuclear and electron recoil events. This allows the neutrino background to be split into a low and high energy regime, such that two separate limits can be set. In the low

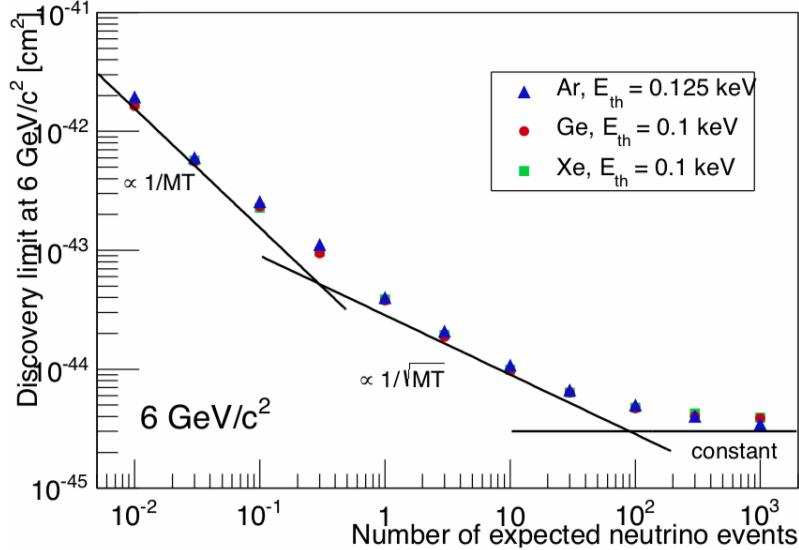


Figure 14: Discovery limit vs exposure for a $6 \text{ GeV}/c^2$ WIMP with Ge, Xe, Ar for 100 neutrino events in 240, 130, and 430 kg-years. Image from [92].

energy regime most events are expected to come from electron recoils. For an neutrino to induce a similar signal it has to have a low momentum. Three sources can create these neutrinos [101]: the solar $p\bar{p}$ -chain, the ^{7}Be decay and double β decay of Xenon-136 [102]. However, their signal is completely different than that of the WIMP-electron scattering. Therefore, it would still be possible to distinguish the WIMP from the background. Eventually, even this background becomes too big and a minimum cross section will be of the order 10^{-48}cm^2 [103].

For the nuclear recoil events the neutrinos need to have a higher energy and their energy spectrum is different. The largest contribution comes from ^{8}B process in the sun [104], which is complemented with neutrinos from the He- p process and a diffuse supernova background. These interactions have a relatively low recoil energy. It is the neutrinos from atmospheric neutrinos that contribute to the background at higher recoil energies. In figure 16 several WIMP masses with a cross section are plotted to show the difference between their event rates. The $6 \text{ GeV}/c^2$ WIMP is almost completely hidden by the solar neutrino background. Therefore, it will be almost impossible to distinguish the signal from the background. Therefore, a expected limit of $10 - 49\text{cm}^2$ has been set for WIMP masses above $10 \text{ GeV}/c^2$. While it would be possible to measure the slight difference between two, it would take unrealistically long as explained in the beginning of this section.

While the limits on the cross section and mass can be decreased to values

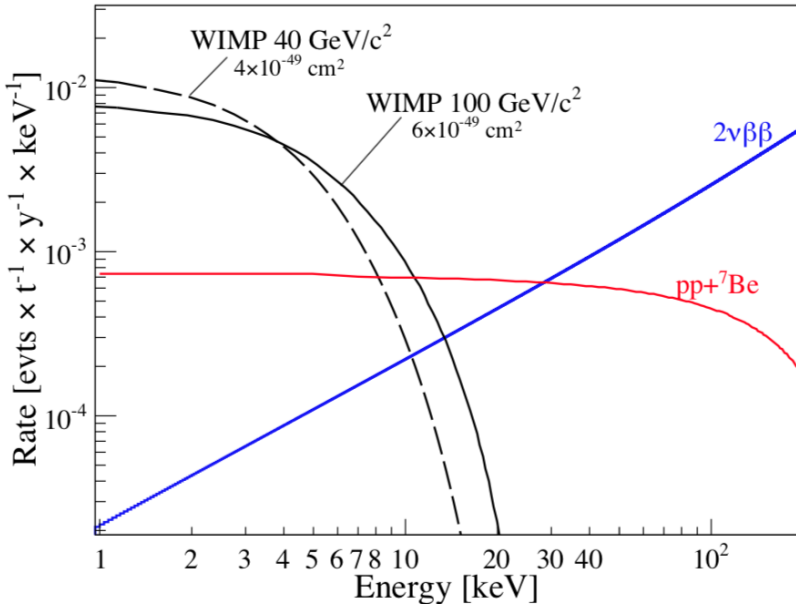


Figure 15: pp , ${}^7\text{Be}$, and double β decay neutrinos scattering of the electron in an LXe detector. The WIMP scattering rate is depicted in black for two different WIMP masses with different cross sections. Image from [101].

below the neutrino floor, eventually no extra parameter space can be reached using current detectors. The exposure will have to be unrealistically large for small cross section and low WIMP mass. This makes it impossible to continue the search using current detectors.

6.3 Continue searching? $J\nu U$

Direct detection experiments are getting bigger in size and improving in sensitivity for the past couple of years. This means that in the nearby future we will probably reach the neutrino floor, explained in the previous section. This will make the detection for WIMPs even harder, because the scattering interaction events of neutrinos in the detector can be equivalent to a WIMP interaction. Therefore it's important to understand if it's possible to distinguish the neutrino background events from the dark matter particles. One important step is to better understand the theoretical estimation of the neutrino fluxes. As well as a better measurement to distinguish the different neutrinos entering the detector.

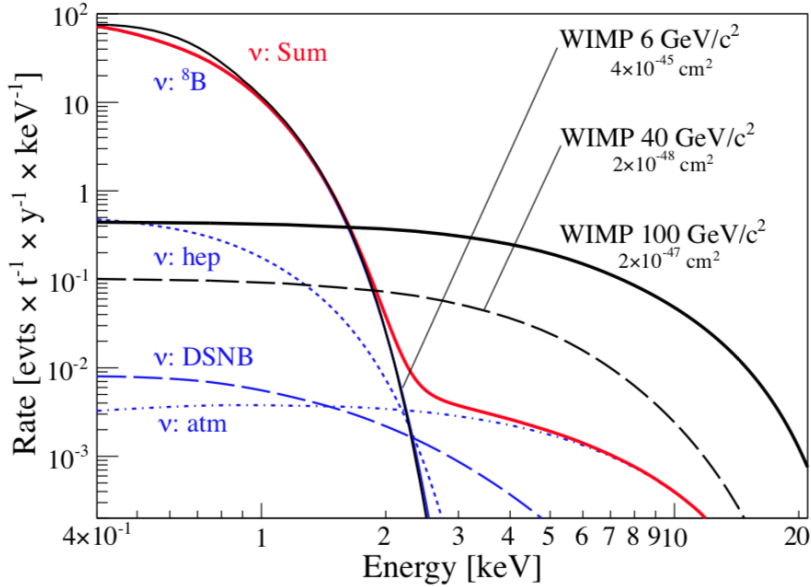


Figure 16: Neutrino scatterings of a nucleus in a LXe detector with the higher energetic solar neutrinos (${}^8\text{B}$) in red, diffuse supernova background (DSNB), He- p , and atmospheric neutrinos in blue. Three WIMP masses have been plotted with different cross sections. Image from [101]

6.3.1 Directional experiments

In the near future new experiments will be available where the nuclear recoil direction can be measured [105]. This is first step in distinguishing neutrinos from WIMPs inside the detector. As described before, most neutrinos are incident from the Sun [92]. As the Earth rotates around its axis every 24 hours, the incoming direction of solar neutrinos will constantly and periodically change. This daily modulation gives a good opportunity to distinguish them from WIMPs, since WIMPs will have a different direction and won't have such a periodic change.

6.3.2 Annual modulation

The DAMA/NaI and DAMA/LIBRA experiments were the first experiment that claimed to have found dark matter [106]. These results showed an annual modulation of the interaction events which was the highest in June (see figure 17). This modulation is a result of the Earth moving faster in the summer and therefore the recoil energy of WIMPs is higher in June.

However, the mass ranges of these WIMPs they claimed to have found, are already ruled out by experiments like XENON1T. This means figure 17 shows

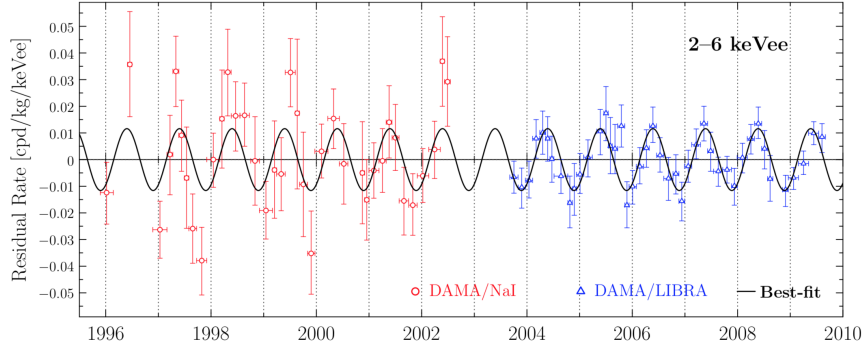


Figure 17: The DAMA/LIBRA experiments claimed to be the first to find a positive dark matter signal. This signal showed an annual modulation over the course of 13 years, which peaked in June. This modulation had a maximum spreading of 6% [106].

false results. But such annual modulations for lower mass ranges might be possible, so similar experiments can still useful in the future.

6.3.3 Extraction of neutrino background

Besides different incoming directions and annual modulation of WIMPs and neutrinos, there will always be some neutrino scattering events which will be similar to those of WIMPs. Therefore it is useful to investigate the how a neutrino only distribution would look like, thus a reconstruction of the neutrino background. In the left graph of figure 18 you can see a simulated distribution of neutrinos in the range where they could mimic the WIMPs [92]. This simulation is done with Xenon as target nucleus. The legend shows the different origin of neutrinos. The left top of the figure, low mass with high cross section, consist mostly of neutrinos that are incident from the Sun. This is different for atmospheric and diffuse supernova neutrino background (DSNB), which have a higher mass and lower energy (bottom right). The right graph of this figure shows an accumulation of all the different neutrinos. However, this time a simulation is done with different target nuclei: Xenon, Germanium, Argon, Silicon, Neon and Fluorine. Again, it's obvious that the solar neutrinos (low mass, high cross section) are the most abundant. Xenon and Germanium, which are heaviest of the target nuclei, also show a non-negligible amount of events for atmospheric and SN neutrinos.

These two graphs show some valuable simulated data. The different target nuclei give slightly different signals. Hence, these target nuclei could be used to distinguish the neutrino background from the WIMPs.

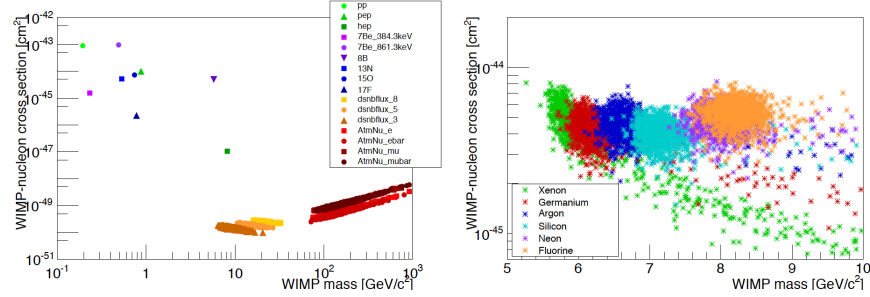


Figure 18: This figure is a numerical simulation of neutrino events, which can mimic the Wimp events. On the left you can see the different neutrino components (solar, atmospheric etc.) with a Xenon nucleus as the target nucleus. The right graph shows the accumulation of all neutrinos. The different color are different target nuclei (Xe, Ge, Ar, Si, Ne, F). [92]

References

- [1] P. A. R. Ade et al. Planck 2015 results. XIII. Cosmological parameters. *Astron. Astrophys.*, 594:A13, 2016.
- [2] J. D. Lewin and P. F. Smith. Review of mathematics, numerical factors, and corrections for dark matter experiments based on elastic nuclear recoil. *Astropart. Phys.*, 6:87–112, 1996.
- [3] David N. Spergel. The Motion of the Earth and the Detection of Wimps. *Phys. Rev.*, D37:1353, 1988.
- [4] Teresa Marrodán Undagoitia and Ludwig Rauch. Dark matter direct-detection experiments. *J. Phys.*, G43(1):013001, 2016.
- [5] Richard H. Helm. Inelastic and Elastic Scattering of 187-Mev Electrons from Selected Even-Even Nuclei. *Phys. Rev.*, 104:1466–1475, 1956.
- [6] G. Fricke, C. Bernhardt, K. Heilig, L. A. Schaller, L. Schellenberg, E. B. Shera, and C. W. de Jager. Nuclear Ground State Charge Radii from Electromagnetic Interactions. *Atom. Data Nucl. Data Tabl.*, 60:177–285, 1995.
- [7] L. Vietze, P. Klos, J. Menéndez, W. C. Haxton, and A. Schwenk. Nuclear structure aspects of spin-independent WIMP scattering off xenon. *Phys. Rev.*, D91(4):043520, 2015.
- [8] G. Co’, V. De Donno, M. Anguiano, and A. M. Lallena. Nuclear proton and neutron distributions in the detection of weak interacting massive particles. *JCAP*, 1211:010, 2012.
- [9] Gintaras Duda, Ann Kemper, and Paolo Gondolo. Model Independent Form Factors for Spin Independent Neutralino-Nucleon Scattering from Elastic Electron Scattering Data. *JCAP*, 0704:012, 2007.
- [10] M. Cannoni. On the formalism and upper limits for spin-dependent cross sections in dark matter elastic scattering with nuclei. *Phys. Rev.*, D84:095017, 2011.
- [11] M. T. Ressell and D. J. Dean. Spin dependent neutralino - nucleus scattering for A approximately 127 nuclei. *Phys. Rev.*, C56:535–546, 1997.
- [12] P. Toivanen, M. Kortelainen, J. Suhonen, and J. Toivanen. Large-scale shell-model calculations of elastic and inelastic scattering rates of lightest supersymmetric particles (LSP) on I-127, Xe-129, Xe-131, and Cs-133 nuclei. *Phys. Rev.*, C79:044302, 2009.
- [13] John R. Ellis and R. A. Flores. Realistic Predictions for the Detection of Supersymmetric Dark Matter. *Nucl. Phys.*, B307:883–908, 1988.

- [14] J. Engel and P. Vogel. Spin dependent cross-sections of weakly interacting massive particles on nuclei. *Phys. Rev.*, D40:3132–3135, 1989.
- [15] Francesco Iachello, Lawrence M. Krauss, and Giuseppe Maino. Spin Dependent Scattering of Weakly Interacting Massive Particles in Heavy Nuclei. *Phys. Lett.*, B254:220–224, 1991.
- [16] D. G. Cerdeno, M. Fornasa, J. H. Huh, and M. Peiro. Nuclear uncertainties in the spin-dependent structure functions for direct dark matter detection. *Phys. Rev.*, D87(2):023512, 2013.
- [17] Nima Arkani-Hamed, Douglas P. Finkbeiner, Tracy R. Slatyer, and Neal Weiner. A Theory of Dark Matter. *Phys. Rev.*, D79:015014, 2009.
- [18] Rouven Essig, Jeremy Mardon, and Tomer Volansky. Direct Detection of Sub-GeV Dark Matter. *Phys. Rev.*, D85:076007, 2012.
- [19] A. Liam Fitzpatrick, Wick Haxton, Emanuel Katz, Nicholas Lubbers, and Yiming Xu. Model Independent Direct Detection Analyses. 2012.
- [20] K. Schneck et al. Dark matter effective field theory scattering in direct detection experiments. *Phys. Rev.*, D91(9):092004, 2015.
- [21] Michael Kuhlen, Neal Weiner, Jurg Diemand, Piero Madau, Ben Moore, Doug Potter, Joachim Stadel, and Marcel Zemp. Dark Matter Direct Detection with Non-Maxwellian Velocity Structure. *JCAP*, 1002:030, 2010.
- [22] Bradley J. Kavanagh, Mattia Fornasa, and Anne M. Green. Probing WIMP particle physics and astrophysics with direct detection and neutrino telescope data. *Phys. Rev.*, D91(10):103533, 2015.
- [23] David G. Cerdeno and Anne M. Green. Direct detection of WIMPs. pages 347–369, 2010.
- [24] Martin C. Smith et al. The RAVE Survey: Constraining the Local Galactic Escape Speed. *Mon. Not. Roy. Astron. Soc.*, 379:755–772, 2007.
- [25] J. Binney and S. Tremaine. *Galactic Dynamics*. Princeton Series in Astrophysics. Princeton University Press, second edition, 2008.
- [26] Lan Zhang, Hans-Walter Rix, Glenn van de Ven, Jo Bovy, Chao Liu, and Gang Zhao. The Gravitational Potential Near the Sun From SEGUE K-dwarf Kinematics. *Astrophys. J.*, 772:108, 2013.
- [27] J. I. Read. The Local Dark Matter Density. *J. Phys.*, G41:063101, 2014.
- [28] Walter Dehnen and Justin Read. N-body simulations of gravitational dynamics. *Eur. Phys. J. Plus*, 126:55, 2011.
- [29] H. Silverwood, S. Sivertsson, P. Steger, J. I. Read, and G. Bertone. A non-parametric method for measuring the local dark matter density. *Mon. Not. Roy. Astron. Soc.*, 459(4):4191–4208, 2016.

- [30] Mark W. Goodman and Edward Witten. Detectability of Certain Dark Matter Candidates. *Phys. Rev.*, D31:3059, 1985. [,325(1984)].
- [31] Christopher McCabe. Prospects for dark matter detection with inelastic transitions of xenon. *JCAP*, 1605(05):033, 2016.
- [32] Carlos E. Yaguna. Isospin-violating dark matter in the light of recent data. *Phys. Rev.*, D95(5):055015, 2017.
- [33] P. Klos, J. Menéndez, D. Gazit, and A. Schwenk. Large-scale nuclear structure calculations for spin-dependent WIMP scattering with chiral effective field theory currents. *Phys. Rev.*, D88(8):083516, 2013. [Erratum: Phys. Rev.D89,no.2,029901(2014)].
- [34] John R. Ellis, R. A. Flores, and J. D. Lewin. Rates for Inelastic Nuclear Excitation by Dark Matter Particles. *Phys. Lett.*, B212:375–380, 1988.
- [35] Glenn D. Starkman and David N. Spergel. A New technique for detecting supersymmetric dark matter. *Phys. Rev. Lett.*, 74:2623–2625, 1995.
- [36] David Tucker-Smith and Neal Weiner. Inelastic dark matter. *Phys. Rev.*, D64:043502, 2001.
- [37] David Tucker-Smith and Neal Weiner. The Status of inelastic dark matter. *Phys. Rev.*, D72:063509, 2005.
- [38] Sen Miao, Chung-Lin Shan, and Yu-Feng Zhou. Model-Independent Identification of Inelastic WIMPs from Direct Dark Matter Detection Experiments. *Int. J. Mod. Phys.*, A29:1450014, 2014.
- [39] R. Foot. A dark matter scaling relation from mirror dark matter. *Phys. Dark Univ.*, 5-6:236–239, 2014.
- [40] Joseph Bramante, Patrick J. Fox, Graham D. Kribs, and Adam Martin. Inelastic frontier: Discovering dark matter at high recoil energy. *Phys. Rev.*, D94(11):115026, 2016.
- [41] R. Agnese et al. First Dark Matter Constraints from SuperCDMS Single-Charge Sensitive Detectors. *Submitted to: Phys. Rev. Lett.*, 2018.
- [42] Douglas P. Finkbeiner, Tongyan Lin, and Neal Weiner. Inelastic Dark Matter and DAMA/LIBRA: An Experimentum Crucis. *Phys. Rev.*, D80:115008, 2009.
- [43] Spencer Chang, Graham D. Kribs, David Tucker-Smith, and Neal Weiner. Inelastic Dark Matter in Light of DAMA/LIBRA. *Phys. Rev.*, D79:043513, 2009.
- [44] Z. Ahmed et al. Search for Weakly Interacting Massive Particles with the First Five-Tower Data from the Cryogenic Dark Matter Search at the Soudan Underground Laboratory. *Phys. Rev. Lett.*, 102:011301, 2009.

- [45] E. Aprile et al. Implications on Inelastic Dark Matter from 100 Live Days of XENON100 Data. *Phys. Rev.*, D84:061101, 2011.
- [46] Sebastian Arrenberg. Search for inelastic dark matter with the CDMS experiment. *PoS*, IDM2010:021, 2011.
- [47] D. Yu. Akimov et al. Limits on inelastic dark matter from ZEPLIN-III. *Phys. Lett.*, B692:180–183, 2010.
- [48] L. Baudis, G. Kessler, P. Klos, R. F. Lang, J. Menéndez, S. Reichard, and A. Schwenk. Signatures of Dark Matter Scattering Inelastically Off Nuclei. *Phys. Rev.*, D88(11):115014, 2013.
- [49] H. Uchida et al. Search for inelastic WIMP nucleus scattering on ^{129}Xe in data from the XMASS-I experiment. *PTEP*, 2014(6):063C01, 2014.
- [50] E. Aprile et al. Search for WIMP Inelastic Scattering off Xenon Nuclei with XENON100. *Phys. Rev.*, D96(2):022008, 2017.
- [51] R. Bernabei et al. Investigating electron interacting dark matter. *Phys. Rev.*, D77:023506, 2008.
- [52] Joachim Kopp, Viviana Niro, Thomas Schwetz, and Jure Zupan. DAMA/LIBRA and leptonically interacting Dark Matter. *Phys. Rev.*, D80:083502, 2009.
- [53] A. Dedes, I. Giomataris, K. Suxho, and J. D. Vergados. Searching for Secluded Dark Matter via Direct Detection of Recoiling Nuclei as well as Low Energy Electrons. *Nucl. Phys.*, B826:148–173, 2010.
- [54] Joseph A. Formaggio, E. Figueroa-Feliciano, and A. J. Anderson. Sterile Neutrinos, Coherent Scattering and Oscillometry Measurements with Low-temperature Bolometers. *Phys. Rev.*, D85:013009, 2012.
- [55] E. Aprile and T. Doke. Liquid Xenon Detectors for Particle Physics and Astrophysics. *Rev. Mod. Phys.*, 82:2053–2097, 2010.
- [56] D. S. Akerib et al. FPGA-based Trigger System for the LUX Dark Matter Experiment. *Nucl. Instrum. Meth.*, A818:57–67, 2016.
- [57] E. Aprile et al. Limits on spin-dependent WIMP-nucleon cross sections from 225 live days of XENON100 data. *Phys. Rev. Lett.*, 111(2):021301, 2013.
- [58] Jianglai Liu. The PandaX Experiment and the Results from the Full Exposure of PandaX-I, 2015.
- [59] Xiangyi Cui et al. Dark Matter Results From 54-Ton-Day Exposure of PandaX-II Experiment. *Phys. Rev. Lett.*, 119(18):181302, 2017.

- [60] Shanghai Jiao Tong University. PandaX: Particle and Astrophysical Xenon Experiments. <https://pandax.sjtu.edu.cn/>.
- [61] Eugenie Samuel Reich. Dark-matter hunt gets deep. *Nature*, 494(7437):291–292, 2013.
- [62] D. S. Akerib et al. Results from a search for dark matter in the complete LUX exposure. *Phys. Rev. Lett.*, 118(2):021303, 2017.
- [63] D. S. Akerib et al. The Large Underground Xenon (LUX) Experiment. *Nucl. Instrum. Meth.*, A704:111–126, 2013.
- [64] Sarah Tesh. Dark-matter constraints tightened after LUX no-shows, 2017. <https://physicsworld.com/a/dark-matter-constraints-tightened-after-lux-no-shows/>.
- [65] E. Aprile et al. Dark Matter Search Results from a One Tonne×Year Exposure of XENON1T. 2018.
- [66] Rafael Lang. Construction started, 2011. <http://www.physics.purdue.edu/darkmatters/xenon1t/?p=192>.
- [67] P. Agnes et al. Results from the first use of low radioactivity argon in a dark matter search. *Phys. Rev.*, D93(8):081101, 2016.
- [68] P. Agnes et al. Status and Perspective of the DarkSide Experiment at LNGS. *Nuovo Cim.*, C40(5):164, 2018.
- [69] E. Edkins et al. The DarkSide direct dark matter search with liquid argon. *AIP Conf. Proc.*, 1900(1):040004, 2017.
- [70] R. Agnese et al. Search for Low-Mass Weakly Interacting Massive Particles Using Voltage-Assisted Calorimetric Ionization Detection in the SuperCDMS Experiment. *Phys. Rev. Lett.*, 112(4):041302, 2014.
- [71] R. Agnese et al. Search for Low-Mass Weakly Interacting Massive Particles with SuperCDMS. *Phys. Rev. Lett.*, 112(24):241302, 2014.
- [72] R. Agnese et al. New Results from the Search for Low-Mass Weakly Interacting Massive Particles with the CDMS Low Ionization Threshold Experiment. *Phys. Rev. Lett.*, 116(7):071301, 2016.
- [73] SuperCDMS Queen’s. http://cdms.phy.queensu.ca/Public_Docs/SuperCDMS_home.html.
- [74] G. Angloher et al. Results on light dark matter particles with a low-threshold CRESST-II detector. *Eur. Phys. J.*, C76(1):25, 2016.
- [75] M. Bravin et al. The CRESST dark matter search. *Astropart. Phys.*, 12:107–114, 1999.

- [76] G. Angloher et al. Results on low mass WIMPs using an upgraded CRESST-II detector. *Eur. Phys. J.*, C74(12):3184, 2014.
- [77] F. Petricca et al. First results on low-mass dark matter from the CRESST-III experiment. In *15th International Conference on Topics in Astroparticle and Underground Physics (TAUP 2017) Sudbury, Ontario, Canada, July 24-28, 2017*, 2017.
- [78] Cresst picture gallery. <https://www.cresst.de/pictures.php>.
- [79] Jianglai Liu, Xun Chen, and Xiangdong Ji. Current status of direct dark matter detection experiments. *Nature Phys.*, 13(3):212–216, 2017.
- [80] APPEC. XENON1T probes deeper into Dark Matter WIMPs, with 1300 kg of cold Xe atoms, 2018. <http://www.appec.org/news/xenon1t-probes-deeper-into-dark-matter-wimps-with-1300-kg-of-cold-xe-atoms>.
- [81] J. Aalbers et al. DARWIN: towards the ultimate dark matter detector. *JCAP*, 1611:017, 2016.
- [82] D. S. Akerib et al. LUX-ZEPLIN (LZ) Conceptual Design Report. 2015.
- [83] B. J. Mount et al. LUX-ZEPLIN (LZ) Technical Design Report. 2017.
- [84] Rouven Essig, Aaron Manalaysay, Jeremy Mardon, Peter Sorensen, and Tomer Volansky. First Direct Detection Limits on sub-GeV Dark Matter from XENON10. *Phys. Rev. Lett.*, 109:021301, 2012.
- [85] Rouven Essig, Mukul Sholapurkar, and Tien-Tien Yu. Solar Neutrinos as a Signal and Background in Direct-Detection Experiments Searching for Sub-GeV Dark Matter With Electron Recoils. *Phys. Rev.*, D97(9):095029, 2018.
- [86] J. Angle et al. A search for light dark matter in XENON10 data. *Phys. Rev. Lett.*, 107:051301, 2011. [Erratum: *Phys. Rev. Lett.* 110, 249901(2013)].
- [87] B. Edwards et al. Measurement of single electron emission in two-phase xenon. *Astropart. Phys.*, 30:54–57, 2008.
- [88] A. Aguilar-Arevalo et al. Search for low-mass WIMPs in a 0.6 kg day exposure of the DAMIC experiment at SNOLAB. *Phys. Rev.*, D94(8):082006, 2016.
- [89] Mariangela Settimo. The DAMIC experiment at SNOLAB. In *53rd Rencontres de Moriond on QCD and High Energy Interactions (Moriond QCD 2018) La Thuile, Italy, March 17-24, 2018*, 2018.
- [90] Michael Crisler, Rouven Essig, Juan Estrada, Guillermo Fernandez, Javier Tiffenberg, Miguel Sofo haro, Tomer Volansky, and Tien-Tien Yu. SENSEI: First Direct-Detection Constraints on sub-GeV Dark Matter from a Surface Run. 2018.

- [91] Jocelyn Monroe and Peter Fisher. Neutrino Backgrounds to Dark Matter Searches. *Phys. Rev.*, D76:033007, 2007.
- [92] J. Billard, L. Strigari, and E. Figueroa-Feliciano. Implication of neutrino backgrounds on the reach of next generation dark matter direct detection experiments. *Phys. Rev.*, D89(2):023524, 2014.
- [93] R. Bonventure and G. D. Orebí Gann. Sensitivity of a low threshold directional detector to CNO-cycle solar neutrinos. *Eur. Phys. J.*, C78(6):435, 2018.
- [94] Y. Fukuda et al. Evidence for oscillation of atmospheric neutrinos. *Phys. Rev. Lett.*, 81:1562–1567, 1998.
- [95] Thomas K. Gaisser. Atmospheric Neutrinos. *J. Phys. Conf. Ser.*, 718(5):052014, 2016.
- [96] Georg G Raffelt. *Stars as laboratories for fundamental physics*. University of Chicago press, 1996.
- [97] John F. Beacom. The Diffuse Supernova Neutrino Background. *Ann. Rev. Nucl. Part. Sci.*, 60:439–462, 2010.
- [98] Y. Totsuka et al. Observation of a neutrino burst from the supernova SN1987a. *Nucl. Phys.*, A478:189–195, 1988.
- [99] A. Gutlein et al. Solar and atmospheric neutrinos: Background sources for the direct dark matter search. *Astropart. Phys.*, 34:90–96, 2010.
- [100] Jason Wyenberge and Ian M. Shoemaker. Mapping the neutrino floor for direct detection experiments based on dark matter-electron scattering. *Phys. Rev.*, D97(11):115026, 2018.
- [101] L. Baudis, A. Ferella, A. Kish, A. Manalaysay, T. Marrodan Undagoitia, and M. Schumann. Neutrino physics with multi-ton scale liquid xenon detectors. *JCAP*, 1401:044, 2014.
- [102] J. B. Albert et al. Search for $2\nu\beta\beta$ decay of ^{136}Xe to the 0_1^+ excited state of ^{136}Ba with EXO-200. *Phys. Rev.*, C93(3):035501, 2016.
- [103] Marc Schumann, Laura Baudis, Lukas Bütkofer, Alexander Kish, and Marco Selvi. Dark matter sensitivity of multi-ton liquid xenon detectors. *JCAP*, 1510(10):016, 2015.
- [104] Louis E. Strigari. Neutrino Coherent Scattering Rates at Direct Dark Matter Detectors. *New J. Phys.*, 11:105011, 2009.
- [105] S. Ahlen et al. The case for a directional dark matter detector and the status of current experimental efforts. *Int. J. Mod. Phys.*, A25:1–51, 2010.
- [106] Katherine Freese, Mariangela Lisanti, and Christopher Savage. Colloquium: Annual modulation of dark matter. *Rev. Mod. Phys.*, 85:1561–1581, 2013.